Generation of hard x-rays by a forsterite terawatt laser

Mikhail B. Agranat*, Nikolay E. Andreev*, Sergei I. Ashitkov*, Edward Boyle[c], Vladimir E. Fortov*, Larry V. Knight [bc], Andrey V.Ovchinnikov*, Alexander P. Shevelko[a]*[c], Dmitry S. Sitnikov*

*Institute for High Energy Densities, Associated Institute for High Temperatures;
[a]Optical Div., P.N.Lebedev Physical Institute; [b]Dept. of Physics and Astronomy, BYU;
[c]Setpoint Spectrometers

ABSTRACT

A compact, tabletop terawatt forsterite laser (1.24 μm /100 mJ/ 80 fs) is used for generation of fast hard x-ray radiation from laser-produced plasmas. Plasmas are created on massive solid Fe and Cu targets. X-ray radiation is studied using a focusing crystal von Hamos spectrometer with a CCD linear array as x-ray detector. High efficiency of the spectrometer in a wide spectral range allows us to record x-ray spectra by one laser shot. Intense K_α radiation is studied with high spectral resolution ($\lambda/\delta\lambda$~1000) at various focusing conditions: main laser radiation and second harmonic radiation. With a copper target the K_α radiation yield was equal to $4\cdot10^9$ photon/pulse in 4π steradian, that corresponds to conversion efficiency of 0.02%**.** Processes responsible for ultrafast hard x-ray radiation are discussed.

Keywords: x-ray spectroscopy, femtosecond laser-generated plasmas

1. INTRODUCTION

The interaction of high intensity femtosecond laser pulses with matter is important both for fundamental research and practical applications. In particular, generation of hot electrons and ultra fast x-ray pulses from femtosecond laser-produced plasmas is a subject of intensive study for the past decade. The ultra fast pulses of characteristic x-ray radiation are used for investigation of phase-transition dynamics, high speed processes, and kinetics of chemical reactions, in biology and medicine (see, for example, reviews[1-6]).

Ti:S femtosecond lasers are commonly used laser systems for this investigation. In this work we report the study of characteristics x-ray radiation from plasmas created by a terawatt forsterite femtosecond laser system of infrared spectral range (λ=1240 nm). High-resolution x-ray characteristic *K*- spectra were recorded using high efficiency focusing crystal spectrometer for one - several laser shots.

*Mikhail B. Agranat. Institute for High Energy Densities, Associated Institute for High Temperatures of the RAS, Izhorskaya, 13/19, Moscow, 125412, Russia, Tel/fax +7 (095) 362 7788, email: utpr@iht.mpei.ac.ru

[a]Alexander Shevelko. Optical Division, P.N.Lebedev Physical Institute of the RAS, Leninsky Pr.53, Moscow 117924, Russia. Tel. +7 095 1326951, fax +7 095 135 2408, e-mail: ashev@sci.levedev.ru

Laser-Generated, Synchrotron, and Other Laboratory X-Ray and EUV Sources, Optics, and Applications II Edited by Kyrala, Gauthier, MacDonald, Khounsary
Proc. of SPIE Vol. 5918, 59180O, (2005) · 0277-786X/05/$15 · doi: 10.1117/12.619631

Downloaded From: http://proceedings.spiedigitallibrary.org/ on 03/27/2014 Terms of Use: http://spiedl.org/terms

2. EXPERIMENT

2.1. The laser system

The experiments were performed using a TW Cr: forsterite (Cr: FOR) CPA femtosecond laser (Fig.1). The system consists of seed oscillator, stretcher, ring regenerative amplifier, power amplifier and compressor. It provides pulses of 80 fs duration, 100 mJ energy at 10 Hz repetition rate with intensity contract better than 10^6 ([7]). All Cr: FOR CPA laser systems, reported previously,[8, 9] had oscillator - regenerative amplifier configuration and their output energy level didn't exceed 0.5 mJ. The stretcher consisted of a single gold-coated 600 grooves/mm grating, dielectric plane and dielectric curve mirror with focal length of 75 cm, which served as one-to-one telescope to change the sign of dispersion. The stretcher extended pulse duration of oscillator up to 90 ps with a total efficiency of ~ 60%.

Stretched pulses were injected into a ring regenerative amplifier cavity. It contains two concave mirror with 70 cm radius of curvature and two flat mirrors. Due to the ring cavity of regenerative amplifier the Faraday optical isolator was not used. The Pockels cell used linear electro-optic effect in KD*P crystal. The Q-switched pump laser (Solar LQ-129-M) had a pulse duration of 12 ns, energy of 15 mJ and operated in the TEM_{00} mode at 10 Hz repetition rate. The on-axis pump fluence achieved 3.1 J/cm^2. The output pulse energy of 450 μJ corresponds to an amplification factor of 3×10^5. The high power amplifier system consisted of four stages of multipass amplifiers. The crystals were pumped by two Q-switched Nd: YAG lasers (Solar LQ-129) at 10 Hz repetition rate with output pulse energy 0.6 J each at λ=1.064 μm. The diameter and divergence of seed beam between stages was corrected by means of the Galilean telescopes, so that, fluence of seed beam was below saturation fluence of 0.8 J/cm^2 and threshold for nonlinear phase distortion. The main parameters of the stages are given in Table 1.

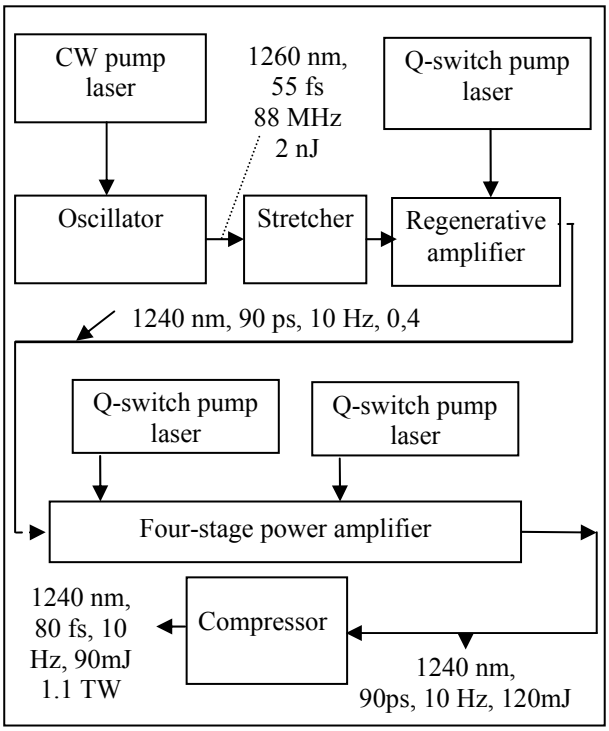


Fig.1. Scheme of the terawatt Cr: forsterite CPA laser system.

Downloaded From: http://proceedings.spiedigitallibrary.org/ on 03/27/2014 Terms of Use: http://spiedl.org/terms

Table 1. The main parameters of the four stages power amplifier.

Amplifier	Number of Passes	Pump Energy, mJ	Output Energy, mJ
1	6	90	6.5
2	4	180	23
3	3	250	47
4	2	600	120

The pulses after high-power amplification were collimated to a diameter of about 30 mm and were compressed with a Treasy-type two-grating compressor. The 600 grooves/mm gold-coated gratings had dimensions of 120×100 mm. The measured throughput efficiency of the compressor was 74%.

Spectra of the compressed and seed pulses are shown in Fig.2. The spectral width (FWHM) of compressed pulses and pulses after oscillator were 26 nm and 50 nm respectively.

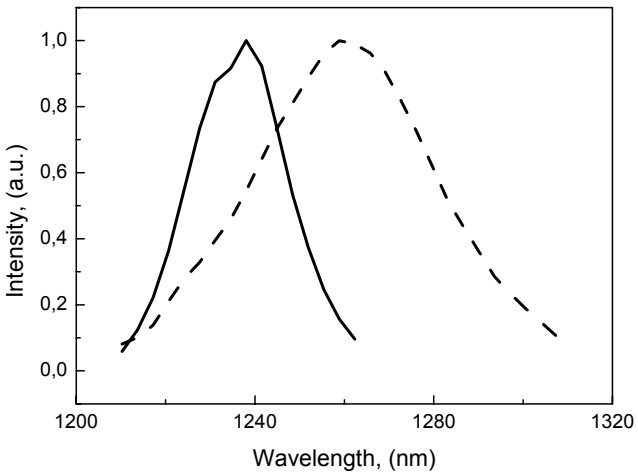


Fig.2. Spectra of the compressed pulse (solid line) and pulse of oscillator (dashed line).

The single-shot autocorrelation trace of the attenuated compressed pulse is shown in Fig.3. The correspondent pulse duration (FWHM) was equal to 80 fs.

Downloaded From: http://proceedings.spiedigitallibrary.org/ on 03/27/2014 Terms of Use: http://spiedl.org/terms

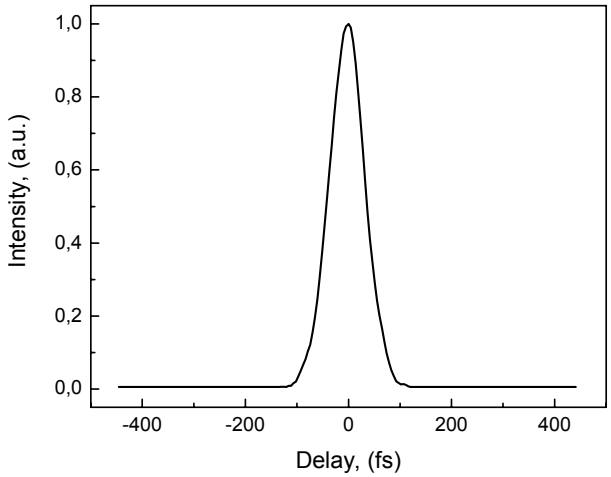


Fig.3. The single-shot autocorrelation trace of the compressed pulse.

High-dynamic range cross-correlation function was measured by third-harmonic cross-correlator and is shown in Fig.4. The intensity contrast of pulses was approximately 10^{-4} at ±1 ps and better than 10^{-6} at ±2 ps.

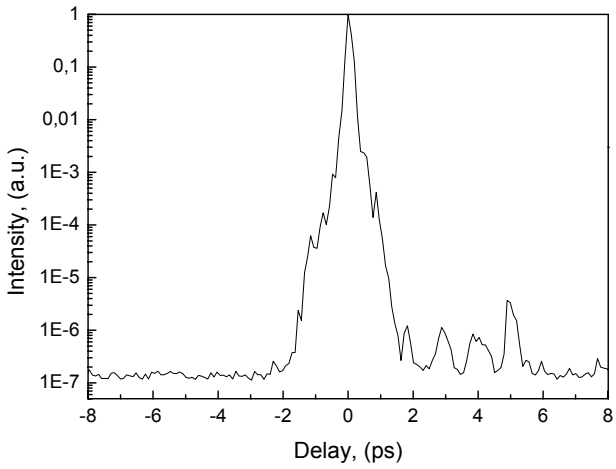


Fig.4. High-dynamic range cross-correlation function.

2.2. Target chamber

The scheme of experiment is shown in Fig. 5. Massive Fe and Cu targets were installed inside a vacuum chamber (10^{-3} torr) on a precision three translations table. Targets were rotated to use a clean surface after each laser shot. Laser radiation was focused onto a target by aberration corrected, antireflection coated three lens objectives with a focal length of 100 mm.

Downloaded From: http://proceedings.spiedigitallibrary.org/ on 03/27/2014 Terms of Use: http://spiedl.org/terms

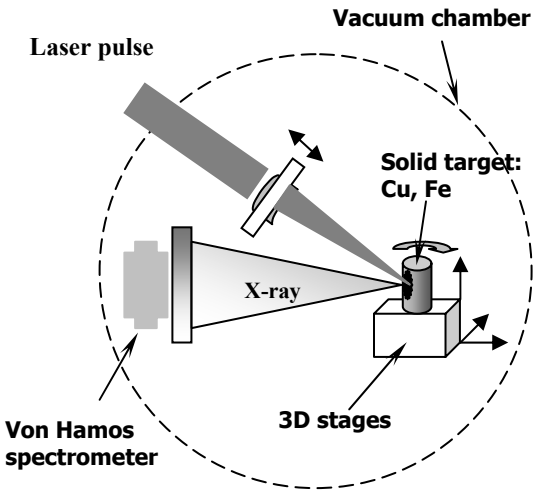


Fig.5. Scheme of experiment.

The angle between laser beam and target normal was 45°. The main frequency (*p*-polarization) and second harmonic (*s*-polarization, λ=620 nm) of laser radiation were used in experiments. Focal spot distribution was measured using a CCD camera.

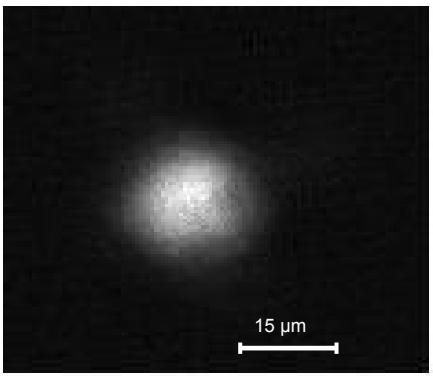


Fig. 6. Focal spot image.

Downloaded From: http://proceedings.spiedigitallibrary.org/ on 03/27/2014 Terms of Use: http://spiedl.org/terms

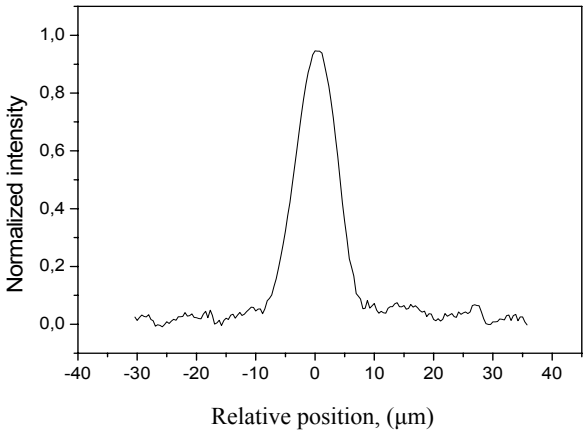


Fig. 7. Intensity distribution in the focal spot.

Image and intensity distribution in the focal spot are shown in Figs.6 and 7. Focal spot diameter was equal to 10 μm that corresponds to maximal laser intensity on the target up to 10^{18} W/cm^2.

2.3. X-ray spectrometer

X-ray characteristic spectra were investigated using the focusing crystal von Hamos spectrometer. In the von Hamos scheme[9, 10] the crystal is bent to a cylindrical surface. The x-ray source and the detector plane lie on the cylinder axis (see Fig. 8). The crystal diffracts x-rays with different wavelengths according to the Bragg law. Each wavelength, after diffraction from the crystal arc, is focused to a point lying on the spectrometer axis. This focusing geometry gives high spectrometer efficiency in a wide spectral range. Another spectrometer advantage is that in the von Hamos geometry x-ray spectra are formed on the spectrometer axis. Thus, it is a possible to use a long length CCD linear array as an x-ray detector to cover a wider spectral range.[11] Earlier this type of spectrometer was actively used for x-ray diagnostics of nanosecond laser-produced plasmas.[10, 11]

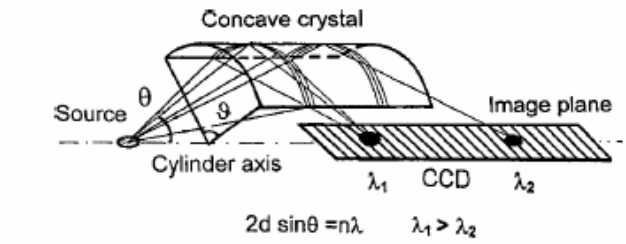


Fig.8. Schematic diagram of the von Hamos spectrometer.

Mica crystal (2*d*=19.84 Å) with radius of curvature *R*=20 mm was used in the spectrometer. The spectrometer was installed in a standard optical mount (Fig. 6). The spectrometer axis was oriented perpendicular to the laser beam (Fig. 5). X-ray characteristic spectra were recorded using the absolutely calibrated CCD positioned in the image plane.[11] The commercial CCD used for x-ray detection is the Toshiba model TCD 1304AP. It is a linear array with 3724 pixels. Each pixel is 8 μm wide (6 μm active) and 200 μm high. The total effective detecting area is 200 μm by 29.8 mm (8 μm x 3724 elements). The front cover glass is removed for x-ray detection. At a temperature of 20° C with an integrating time of 100 ms, the dark current noise, 3σ, is 0.5 % of the saturation value. To prevent visible light illumination, a double Al-coated mylar filter (4.4 μm of mylar, 0.2 μm of Al) was used. The focusing geometry of the crystal also as high CCD

Downloaded From: http://proceedings.spiedigitallibrary.org/ on 03/27/2014 Terms of Use: http://spiedl.org/terms

sensitivity leads to a very high device efficiency: focusing intensities could be 10^4-10^6 times higher than those of flat crystal spectrometers with photographic film registration.[11]

X-ray spectra were recorded in the fifth diffraction order of the mica crystal for one – several laser shots. This gives a possibility to perform x-ray spectra monitoring in a real time scale. Absolute spectrometer calibration allowed the use of an absolutely intensity scale (see Fig. 9-11) and to determine absolute radiation yield (proposed isotropic source). Due to the high spectral resolution ($\lambda/\delta\lambda \approx 500$-$1000$) it was possible to observe complete spectral structure: K_α and K_β characteristic lines.

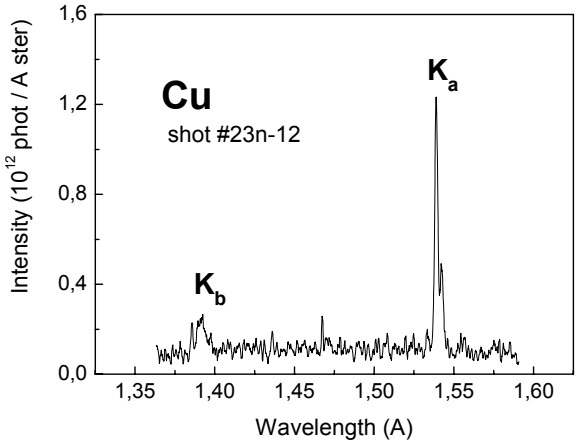


Fig. 9. Overview spectrum of Cu target (angle of incidence 45º, main frequency ω_0, 20 laser shots, pulse energy E_L=30 mJ).

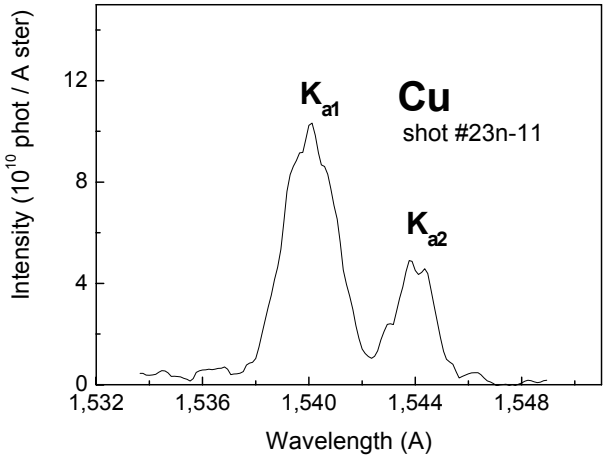


Fig.10. Spectrum of Cu target (angle of incidence 45º, main frequency ω_0, one laser shot, pulse energy E_L=30 mJ, spectral resolution – $\lambda/\delta\lambda$=1000).

Downloaded From: http://proceedings.spiedigitallibrary.org/ on 03/27/2014 Terms of Use: http://spiedl.org/terms

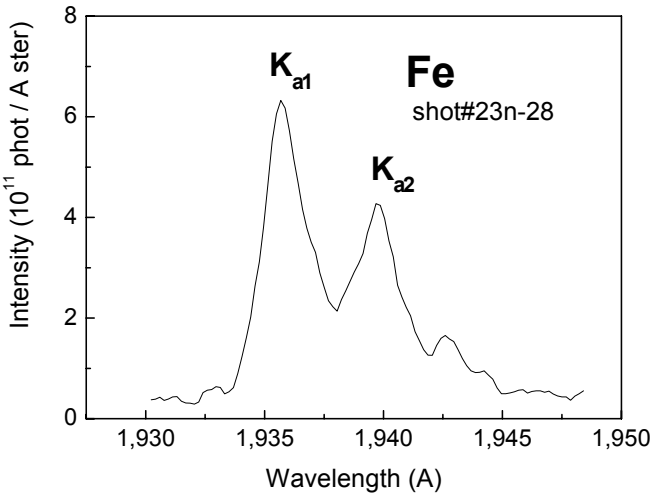


Fig.11. Spectrum of Fe target (angle of incidence 45º, main frequency ω_0, 10 laser shots, pulse energy E_L=15 mJ, spectral resolution – $\lambda/\delta\lambda$=850).

3. RESULTS AND DISCUSSIONS

Absolute radiation yield X (phot/ster pulse) and conversion efficiency $\eta=E_{x\text{-}ray}/E_L$ of laser radiation into x-ray radiation: $K_\alpha = K_{\alpha 1} + K_{\alpha 2}$ are presented in Table 2. Maximal conversion efficiency was achieved with values of η=0.02 % that exceeds values of similar measurements in refs.[12-15]

Table2. Absolute radiation yield X (phot/ster pulse) and conversion efficiency $\eta=E_{x\text{-}ray}/E_L$ at different focusing conditions.

Focusing conditions	E_L, mJ	X (phot/ster pulse)	$\eta = E_{x\text{-}ray} / E_L$
Cu, ω_0, p-polarization	5	8.3×10^{7}	2.6×10^{-4}
	30	3.3×10^{8}	1.8×10^{-4}
Cu, $2\omega_0$, s-polarization	5	1.1×10^{7}	3.6×10^{-5}
Fe, ω_0, p-polarization	5	3.3×10^{7}	8.2×10^{-5}
	15	2.1×10^{8}	1.6×10^{-4}
Fe, $2\omega_0$, s-polarization	5	3.1×10^{6}	7.8×10^{-6}

To describe a short intense laser pulse interaction with solid targets the two temperature hydro model was used with allowance made for the processes of the pump laser pulse absorption, ionization and heating of the target matter, ponderomotive pressure of the laser radiation, and also accomplished by the Maxwell equations for the heating laser pulse.[16, 17]

Downloaded From: http://proceedings.spiedigitallibrary.org/ on 03/27/2014 Terms of Use: http://spiedl.org/terms

The results of modelling showed that the maximum temperature of the main part of electrons is in the range of 350÷700 eV for the parameters of the experiment. The high contrast of the pump laser pulses causes a small characteristic scale length of the produced plasma density, which in the range of intensities of the current experiment, $I_L \approx (0.5 \div 3) \times 10^{17}$, was about a few nanometers during the time of the laser pulse action. In this case for a p-polarized laser pulse the amplitude of electron oscillations in the normal to the target component of the laser field was much higher than the scale of the plasma density inhomogeneity that provides an effective generation of hot electrons due to its "vacuum heating". [18] The temperature of the hot electrons can be estimated by the relation

$$T_{hot} \approx 74\, I_L\, \lambda_L^2 \sin^2\theta\,,$$

where λ_L is the laser wavelength in nm, I_L is measured in 10^{17} W/cm^2 and θ is the angle of incidence of *p*-polarized radiation to the target. For parameters of our experiments this estimation gives the values of hot electrons temperature in the range of a few tens of keV that corresponds to the energies necessary to generate K_α radiation measured in the experiment. These carried our investigations of K_α radiation from the plasma produced by the femtosecond laser in near infrared range with the high time contrast of pulses show the efficient conversion of laser radiation to X-rays. For the case of *p*-polarized laser pulses obtained results indicate the determining role of "vacuum heating" of hot electrons, which are responsible for generation of K_α radiation.

ACKNOWLEDGEMENTS

The research was supported by the Presidium of Russian Academy of Sciences in the frame of Programs for Basic Research # 2 and # 16 and by the Russian Foundation for Basic Research, grant 04-02-17055.

REFERENCES

1. P. Gibbon, E. Forster, "Short-pulse laser-plasma interactions," Plasma Phys. Control. Fusion, **38** (6), 769-793, 1996.
2. Ch. Reich, P. Gibbon, I. Uschmann, E. Forster, "Yield Optimization and Time Structure of Femtosecond Laser Plasma *K alpha* Sources," *Phys. Rev. Lett*., **84**, 4846-4849, 2000.
3. A. Rousse, C. Rischel, J. -C. Gauthier, "Femtosecond x-ray crystallography," Rev. Modern Physics, **73**, 17-31, 2001.
4. D. Von der Linde, K. Sokolowski-Tinten, Ch. Blome, et al, "Generation and application of ultrashort X-ray pulses," Laser and Particle Beams, **19**, 15-22, 2001.
5. D. Umstadter, "Physics and Applications of Relativistic Plasmas Driven by Ultra-intense Lasers," Physics of Plasmas, **8** (5), 1774-1785, 2001.
6. A. Sjögren, M. Harbst, C. -G. Wahlström, S. Svanberg, "High-repetition-rate, hard x-ray radiation from a laser-produced plasma: Photon yield and application considerations," Rev. Sci. Instrum., **74** (4), 2300-2311, 2003.
7. M. B. Agranat, S. I. Ashitkov, A. A. Ivanov, A. V. Konyashchenko, A. V. Ovchinnikov, V. E. Fortov, "Terawatt femtosecond Cr: forsterite laser system," Quantum Electronics**, 34** (6), 506-508, 2004.
8. V. Petrov, F. Noack, and F. Rotermund, "Femtosecond regenerative amplification in Cr: forsterite at 5-10 kHz," Appl. Phys., **B 75**, 791, 2002.
9. Von L.v.Hámos, "Röntgenspektroskopie und Abbildung mittels gekrùmmter Kristallreflektoren", Ann.Phys., **17**, 716-724, 1933.
10. A. P. Shevelko, "X-ray spectroscopy of laser-produced plasmas using a von Hamos spectrograph," Proc. SPIE **3406**, 91-108, 1998.
11. A. P. Shevelko, Yu. S. Kasyanov, O. F. Yakushev, L. V. Knight, "Compact focusing von Hamos spectrometer for quantitative x-ray spectroscopy," Rev. Sci. Instrum., **73**, 3458-3463, 2002.
12. N. Takeyasu, Y. Hirakawa, T. Imasaka, "Emission spectrum of hard x-rays, generated from iron, copper, and molybdenum targets by sub picosecond KrF laser pulses," Appl. Phys. Lett., **78** (9), 1195-1197, 2001.

Downloaded From: http://proceedings.spiedigitallibrary.org/ on 03/27/2014 Terms of Use: http://spiedl.org/terms

13. G. Korn, A. Thoss, H. Stiel, et al, "Ultrashort 1-kHz laser plasma hard x-ray source," Opt. Lett., **27** (10), 866-868, 2002.
14. Y. Jiang, T. Lee, W. Li, et al, "Generation of ultrashort hard-x-ray pulses with tabletop laser systems at a 2-kHz repetition rate," J. Opt. Soc. Am., **B 20** (1), 229-237, 2003.
15. L. M. Chen, P. Forget, S. Fourmaux, et al, "Study of hard x-ray emission from intense femtosecond Ti: sapphire laser–solid target interactions," Physics of Plasmas**, 11** (9), 4439-4445, 2004.
16. N. E. Andreev, V. V. Kostin, M. E. Veisman, "Redistribution of Energy in Dense Matter Irradiated by Short Intense Laser Pulses," Physica Scripta**, 58** (5), 486-492, 1998.
17. N. E. Andreev, M. E. Veisman, V. P. Efremov, V. E. Fortov, "Generation of high density hot plasma by intense subpicosecond laser pulses," High Temperature*,* **41**, 594, 2003.
18. F. Brunel, "Not-So-Resonant, Resonant Absorption," Phys. Rev. Lett.**, 59**, 52-55, 1987.

Downloaded From: http://proceedings.spiedigitallibrary.org/ on 03/27/2014 Terms of Use: http://spiedl.org/terms